

Evaluation of the effect of arabinogalactans extracted from matcha on gamma radiation-induced brain damage in rats

Mohamed Y.M. Awad¹, Eithar K. El Adham², Amal I. Hassan^{2,*} 

ABSTRACT

Introduction: Radiation has adverse effects on brain tissue. Natural products have anti-inflammatory and anti-inflammatory properties. This study investigates the protective effect of alginate extract from matcha against gamma radiation damage. **Methods:** We isolated and characterized arabinogalactans (AG) from matcha powder. We randomly divided thirty-two male rats into four equal groups (n = 8 rats/group). The first group served as the control, while the second group administered MAG orally to the rats for 14 days. The third group of rats underwent a single dose of 10 Gy of head-localized irradiation (Rad). The fourth group, rats, received MAG for 7 days before and after 10 Gy γ irradiation (B & A). We examined the brain for markers of oxidative stress and inflammation. We used immunohistochemistry to monitor tumor necrosis factor alpha (TNF- α), interleukin 1 beta (IL-1 β), interleukin 6 (IL-6), and apoptosis-regulating proteins BAX and BCL2. We measured levels of glutathione (GSH), superoxide dismutase (SOD), catalase (CAT), and malondialdehyde (MDA) in brain tissues as indicators of oxidative stress. Western blot analysis assessed apoptotic markers like cleaved caspase-3 and neurotrophic factors, including Brain-derived neurotrophic factor (BDNF). Additionally, Double Delta Ct QPCR was employed to evaluate gene expression changes in monoamine oxidase (MOA), acetylcholinesterase (AChE), and nuclear factor kappa B (NF- κ B). Histopathological tests were performed to verify the effects of therapy, elucidating neuronal damage and inflammation. **Results:** Radiation exposure elevated oxidative stress indicators, pro-inflammatory cytokines, and apoptotic proteins, while diminishing antioxidant and BDNF levels. The MAG therapy (B & A) decreased MDA levels and pro-inflammatory cytokines (TNF- α , IL-1 β). MAG lowers SOD and GSH levels while enhancing catalase activity. It also altered the concentrations of apoptosis-related proteins such as BAX, BCL2, and cleaved caspase-3. QPCR results indicated that MAG reinstated the modified MAO-A, AChE, and NF- κ B genes. Histological analyses validated the protective properties of MAG, demonstrating decreased tissue injury and inflammation. **Conclusion:** This study demonstrates that matcha-derived arabinogalactans may protect neurons from radiation-induced cerebral injury. This is likely attributable to their antioxidant, anti-inflammatory, and anti-apoptotic characteristics.

Key words: Gamma radiation, Neuroprotection, Oxidative stress, Inflammation, Apoptosis, Antioxidants

¹Al- Azhar University Center for virus Research and Studies, Cairo, Egypt

²Department of Radioisotopes, Nuclear Research Centre, Egyptian Atomic Energy Authority, Egypt

Correspondence

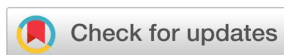
Amal I. Hassan, Department of Radioisotopes, Nuclear Research Centre, Egyptian Atomic Energy Authority, Egypt

Email: virtualaml@gmail.com

History

- Received: Oct 22, 2024
- Accepted: Mar 13, 2025
- Published Online: Mar 31, 2025

DOI : 10.15419/bmrat.v12i3.967



Copyright

© Biomedpress. This is an open-access article distributed under the terms of the Creative Commons Attribution 4.0 International license.



INTRODUCTION

In recent years, the potential health benefits of natural plant extracts have received increasing attention in medical research. Among these compounds, arabinogalactans, a polysaccharide abundant in plant species, seem to have promising therapeutic effects¹. The finely ground powder of mature and processed tea leaves is particularly recognized for its high content of bioactive compounds, including matcha arabinogalactans, making it important to investigate potential radiosafety compounds^{2,3}.

Gamma rays, an ionizing radiation, are widely used in medical research and cancer treatment. However, exposure to gamma rays carries a high risk of oxidative stress, inflammation, and damage to biological tissues, especially the brain^{4,5}. The central nervous system

is extremely sensitive to radiation damage due to its complex cellular structure and metabolic demands. Proteoglycans, or arabinogalactans, are a class of polymers associated with plant growth and development. They are found in many tissues of higher plants, such as the outer cell matrix, cell walls, and plasma membranes, and the larch tree (*Larix sp.*) is considered the most abundant source in the USA⁶. Larch-derived arabinogalactan is recognized as a source of dietary fiber, but it is also believed to have potential therapeutic value as a stimulant in immune and cancer programs⁷. The molecular weight of arabinogalactans typically ranges from 10 kDa to 4000 kDa. Their protein content is usually less than 10%, consisting mainly of proline/hydroxyproline, alanine, serine, and threonine. More than 90% of arabinogalac-

Cite this article : Awad M Y, Adham E K E, Hassan A I. Evaluation of the effect of arabinogalactans extracted from matcha on gamma radiation-induced brain damage in rats. *Biomed. Res. Ther.* 2025; 12(3):7246-7264.

tans are polysaccharides, primarily β -(1-3)-galactan chains with a β -(1-6)-galactosyl side chain, usually terminated by an arabinyl residue⁸. The structural investigation of arabinogalactan-proteins, which are crucial signaling molecules of the plant cell wall, has been widely studied in angiosperms. However, there is a scarcity of information on gymnosperms⁹. Polyphenolic compounds have been shown to affect pro-inflammatory signaling, pro-inflammatory cytokines, and radiation-induced damage. Anti-inflammatory properties of certain compounds, such as anthocyanin, curcumin, and resveratrol, have also been identified as significant radioprotectors^{10,11}. Arabinogalactans possess antioxidant, anti-inflammatory, and immunomodulatory activities that can mitigate the detrimental effects of radiation on cerebral tissue. Moreover, scaffold-derived arabinogalactans offer the advantage of being a simple natural source without adverse effects¹².

Our goal in this study was to investigate the neuroprotective potential of arabinogalactans extracted from matcha against gamma radiation-induced brain damage. Rats are an established model for studying the physiological and pathological effects of radiation on brain function. Using a mouse model, we can better mimic the response to human brain exposure to gamma radiation.

METHODS

AG Extraction and Characterization

Matcha, a powdered green tea, was graciously provided by Hangzhou Shandi Tea Industry Co., Ltd. (Hangzhou, China). The AG was obtained using the Bartle¹³ approach. The dried plant material was subjected to a 24-hour aqueous extraction process at a ratio of 1:10 (w/v) with continuous shaking at 4 °C. The solid plant material was then extracted and heated at 92 °C for 10 minutes. The extract was held overnight at 4 °C to facilitate the precipitation of proteins while ensuring that the AG remained soluble. The proteins were removed by centrifugation at 15,000 g and 4 °C for 10 minutes. To separate a high molecular weight (HMW) fraction rich in polysaccharides and AG proteins, the extract was mixed with cold 100% ethanol until it reached an 83% (v/v) concentration. The precipitate was then subjected to centrifugation at 15,000 g and 4 °C for 20 minutes. The HMW fraction was freeze-dried. The AGP was isolated from the HMW fraction through selective precipitation using β -glucosyl-Yariv reagent (β GlcY), as described by Classen *et al.*¹⁴ and Paulsen *et al.*¹⁵.

High-Performance Liquid Chromatography (HPLC) Analysis

HPLC analysis was performed using an Agilent 1260 series system equipped with a Zorbax Eclipse Plus C8 column (4.6 mm \times 250 mm, 5 μ m particle size). The mobile phase consisted of two components: A (water) and B (0.05% trifluoroacetic acid in acetonitrile). The separation was carried out using a linear gradient elution at a flow rate of 0.9 mL/min as follows: 0–1 min: 82% A, 1–11 min: 75% A, 11–18 min: 60% A, 18–22 min: 82% A, and 22–24 min: 82% A (re-equilibration phase).

The column temperature was maintained at 40 °C. Detection was performed at a wavelength of 280 nm using a multi-wavelength detector. The injection volume for each sample was 5 μ L. Standards of gallic acid and chlorogenic acid were prepared at known concentrations to generate calibration curves. Sample solutions were then analyzed under identical conditions, and their concentrations were determined by interpolating peak areas into the standard calibration curves.

Fourier Transform Infrared (FTIR) Spectroscopy

FTIR analysis was performed to identify the functional groups present in the extracted arabinogalactans. The spectra were recorded using a Bruker VERTEX 80 FTIR spectrometer equipped with a Platinum Diamond ATR accessory. The analysis was conducted in the range of 4000–400 cm^{-1} with a resolution of 4 cm^{-1} . The sample was placed directly on the ATR crystal, ensuring full contact, and spectra were obtained after 16 scans to enhance the signal-to-noise ratio.

The characteristic absorption bands were analyzed to determine the presence of functional groups, including hydroxyl (O-H), carbonyl (C=O), ether (C-O), and glycosidic bonds (C-O-C). The results were compared to known spectra of arabinogalactans for structural confirmation.

Assessment of total phenolic content

Zilic *et al.*¹⁶ assessed the total phenolic content using the Folin-Ciocalteu method. The extract (100 μ L) was placed in a test tube, and distilled water was added to make it 3.5 mL. Next, 250 μ L of Folin-Ciocalteu's reagent was added to start the oxidation process. We added 1.25 mL of 20% aqueous sodium carbonate (Na_2CO_3) solution to the mixture after the reaction to stop it. After waiting for 40 minutes, we measured the absorbance at 725 nm, using the blank as a reference. We quantified the total phenolic content from

the calibration curve using gallic acid and expressed the results in milligrams (mg GAE) per gram of the sample.

Determination of total flavonoid content

The total flavonoid content was determined using the aluminum chloride (AlCl₃) colorimetric method as outlined by Zilic *et al.*¹⁷. In summary, 300 μL of 5% sodium nitrite (NaNO₂) was mixed with 100 μL of extract. After 6 minutes, 300 μL of a 10% AlCl₃ solution was added, and the total volume was adjusted to 2.5 mL with distilled water. After 7 minutes, 1.5 mL of 1 M NaOH was added, followed by centrifugation at 5000 g for 10 minutes. The absorbance of the supernatant was measured at 510 nm for the solvent blank. The total flavonoid concentration was determined using a calibration curve derived from catechin and represented as μg CE/g sample.

Radical DPPH scavenging efficacy

Using the stable 1,1-Diphenyl-2-picryl-hydrazyl (DPPH•), we evaluated the capacity to scavenge free radicals. For this ATR-FTIR study, we used a Bruker VERTEX 80 (Germany) coupled with a Platinum Diamond ATR. A diamond disk with a refractive index of 2.4 and a resolution of 4 cm⁻¹ acts as an internal reflector in this device, operating in the 4000–400 cm⁻¹ range.

The overall reaction volume was 4.0 mL, and the final concentration of DPPH• was 50 μM. After 60 minutes, we measured the absorbance at 517 nm (A) in comparison to a pure methanol blank. The following equation was used to obtain the % inhibition of the DPPH free radical:

$$\text{Calculation of inhibition (\%)} = 100 \times (A_{\text{control}} - A_{\text{sample}}) / A_{\text{control}}$$

The antioxidant activity was measured in micrograms of Trolox equivalent (TE) per gram of material, according to a calibration curve set up with Trolox.

Assessment of ABTS radical scavenging activity

The ABTS radical scavenging activity was evaluated by making stock solutions of the reagent according to the method described by Hwang and Do Thi¹⁸. This involved mixing 7 mM of aqueous ABTS* with 2.45 mM of potassium persulfate in equal volumes, then incubating the mixture for 16 hours at room temperature (25 °C) in the dark. To create a working solution, 1 mL of ABTS* solution was mixed with 60 mL of a 50:50 (v/v) ethanol and water mixture. This mixture was tested using a Spectro UV-VIS

Double Beam spectrophotometer (Model UVD-3500, Labomed, Inc., La Cienega Blvd., Los Angeles, CA 90034, U.S.A.) to ensure an absorbance of 1.0 ± 0.02 units at 734 nm. For one hour in the dark, 50 μL of the extracts were allowed to react with 4.95 mL of the ABTS* solution. Using a spectrophotometer, the absorbance was determined at a wavelength of 734 nm. A standard curve was created using Trolox. Data were shown as micrograms of Trolox equivalents (TE) per gram.

Determination of LD50 of MAG in rats

In drug screening, the measurement of LD₅₀ (the dosage lethal to 50% of the tested animal population) is typically a first step in evaluating the hazardous properties of a chemical. This initial toxicity evaluation offers insights into potential health risks associated with short-term drug exposure and is one of the initial screening tests conducted on all substances^{19,20}. The examined substances were delivered in incremental dosages, and the LD₅₀ was ascertained²¹. We estimated the optimal dose for assessing the *in vivo* antitumor efficacy of the examined drugs to be one-tenth of their LD₅₀ value.

Gamma Irradiation

A Canadian gamma cell 40 (137Cs) at the National Center for Radiation Research and Technology (NCRRT) in Cairo, Egypt was used to irradiate the rats' head only exposure at dose 10 Gy, while the rest of the body was shielded with 5-mm-thick lead. The dose rate was 0.585 rad/sec. Rats were anesthetized via intraperitoneal (IP) injection of sodium pentobarbital (50 mg/kg) to maintain immobility during the irradiation period. The animals were irradiated individually rather than concurrently. Each rat was separately anesthetized, positioned in the gamma cell, and exposed to the radiation source under controlled conditions.

Animal Experiments

We recruited mature male albino rats ranging in weight from 180 to 200 g from the NCRRT's animal house in Cairo, Egypt. We fed the animals a regular pellet diet and provided water ad libitum. We kept them in a controlled environment with a 12-hour light-dark cycle, at room temperature and pressure.

Experimental Groups and Treatment Protocol

A total of 32 male Wistar albino rats, weighing between 180 and 200 grams and aged 6 to 8 weeks, were randomly divided into four groups (n = 8):

- Group 1 (Control): Rats received an oral gavage of 0.9% sodium chloride solution (saline) daily for 14 days.
- Group 2 (MAG): Rats received oral gavage of Matcha-derived arabinogalactans (MAG) at a therapeutic dose daily for 14 days.
- Group 3 (Localized Irradiation): Rats were exposed to 10 Gy gamma radiation targeted to the head using a precise collimator to minimize radiation to other body regions²².
- Group 4 (Pre-MAG + Radiation + Post-MAG): Rats received MAG at the therapeutic dose for 7 consecutive days prior to 10 Gy head-localized gamma radiation, followed by continued administration of MAG for 7 days post-irradiation.

On day 15, animals were anesthetized using intraperitoneal injection of sodium pentobarbital (60 mg/kg) to ensure minimal stress. Blood samples were collected via cardiac puncture. Following blood collection on day 15, animals were humanely euthanized using an overdose of sodium pentobarbital (150 mg/kg) administered intraperitoneally, followed by cervical dislocation to ensure death.

The study was conducted following approval by the Institutional Animal Care and Use Committee (IACUC) of the National Centre for Radiation Research and Technology (NCRRT), Cairo, Egypt, under approval number (permission No P/35A/24) on May 2, 2024. All procedures complied with the ethical guidelines outlined by the National Institutes of Health (NIH) Guide for the Care and Use of Laboratory Animals.

Protein extraction and purification

Rats were sacrificed, and brain tissues were dissected to prepare 10% tissue homogenates in ice-cold phosphate buffer for analysis of oxidative stress and inflammation markers. The TriFast technique (Peqlab, VWR) was used for protein extraction, allowing the simultaneous isolation of RNA, DNA, and protein. Tissue samples (50–100 mg) were homogenized in 1 mL of TriFast using either a Glass-Teflon or power homogenizer, ensuring the sample volume did not exceed 10% of the TriFast solution. After the addition of 0.2 mL of chloroform per 1 mL of TriFast, the mixture was vigorously shaken for 15 seconds and incubated at room temperature for 3–10 minutes. The mixture was then centrifuged at $12,000 \times g$ for 5 minutes. The protein-containing phase was separated and precipitated with 0.5 mL of isopropanol per 1 mL of TriFast,

incubated on ice, and centrifuged at $12,000 \times g$ for 10 minutes at 4°C .

The precipitated protein pellet was washed three times with 0.3 M guanidinium hydrochloride in 95% ethanol, incubated at room temperature for 20 minutes, and centrifuged at $7,500 \times g$ for 5 minutes. The pellet was then mixed with 2 mL of 100% ethanol, incubated for 20 minutes, centrifuged, vacuum-dried, and reconstituted in buffer. Residual insoluble material was removed by additional centrifugation at $10,000 \times g$ for 10 minutes at 4°C . The protein-containing solution was stored at -20°C .

Protein Quantification

Protein concentration was determined using the Bradford method. Each sample (50 μL) was mixed with 50 μL of distilled water and 200 μL of Coomassie Brilliant Blue G-250 reagent. After a 5-minute incubation, absorbance was measured at 595 nm. Protein concentrations were calculated using a BSA standard curve prepared under the same conditions.

Gel Electrophoresis

Acrylamide-bisacrylamide gels were prepared with 12% resolving and 4% stacking layers, following the method of Bamdad et al. Protein samples (30 μg) were loaded onto the gel and separated at 75 V for the stacking layer and 125 V for the resolving layer over 2 hours. The gel was stained with 0.1% Coomassie Blue R-250 in a methanol-acetic acid solution (1:3:6) and destained to visualize the protein bands. Protein bands were visualized using the Geldoc-it system (UVP, England) and analyzed with TotalLab software to determine molecular weight and protein expression.

Molecular Assessments

We prepared blotting buffers for the blotting technique, which consist of 25 mM Tris, pH 7.4, 0.15 M NaCl, and 0.1% Tween 20. We prepared a blocking solution using 2–5% nonfat dry milk, adjusted to a pH of 7.4. We produced an antibody solution in the blotting buffer using dried milk (1–5% fat), then adjusted the solution according to the proteins separated by SDS-PAGE. We transferred these proteins onto Hybond™ nylon membranes (GE Healthcare). β -actin was used as the control protein and was incubated at ambient temperature in the blocking solution for one hour. Next, the membrane was placed in a solution containing an anti-BDNF antibody [EPR1292, Abcam, USA, 15 kDa] and left at 4°C overnight.

Following incubation, the membrane was rinsed with

at least five consecutive replacements of blotting buffer for 30 to 60 minutes at room temperature. After that, the membrane was placed in a solution of an HRP-conjugated secondary antibody diluted appropriately for one hour at room temperature. The antibody concentration was systematically adjusted within the range of 0.05 to 2.0 $\mu\text{g}/\text{mL}$ until the desired signal strength was achieved. Finally, the membrane was rinsed again (five or more times) with blotting buffer for 30–60 minutes.

QPCR Analysis Using Double Delta Ct MAO-A gene expression

TRIzol Reagent (15596026, Life Technologies, USA) was used for total RNA purification from blood samples according to the manufacturer's protocol. TRIzol Reagent's unique combination of phenol, guanidine isothiocyanate, and other components enables the sequential precipitation of RNA, DNA, and proteins from a single sample. After homogenization with TRIzol, chloroform was added to separate the solution into three layers: an aqueous RNA layer, an interphase, and a red organic layer containing DNA and proteins. RNA was then precipitated with isopropanol. DNA was separated from the organic/interphase layer with ethanol, and protein was obtained by isopropanol precipitation.

For RNA extraction, the sample was transferred to a centrifuge tube and treated with RBC Lysis Buffer, then centrifuged. The pellet was washed and resuspended in DPBS, then centrifuged again. TRIzol reagent was added, and the sample was stored at -80°C . After incubation, chloroform was added, and the mixture was centrifuged at $12,000 \times g$ at 4°C for 15 minutes. RNA in the aqueous layer was precipitated with isopropanol, washed with 75% ethanol, air-dried, and resuspended in RNase-free water or buffer. The QuantiTect Reverse Transcription Kit was employed to convert RNA into cDNA, ensuring removal of genomic DNA contamination. The material was incubated at 42°C for reverse transcription, followed by 95°C , and the cDNA was used immediately for PCR or stored at -20°C .

Preparation of quantitative PCR reaction

The Rotor-Gene Q (Qiagen, USA) was utilized to conduct real-time PCR for the evaluation of mRNA levels of AChE and MAO-A genes. β -actin was used as the housekeeping gene. Amplifications were carried out using the Maxima SYBR Green/Fluorescein qPCR Master Mix (2X), which contains SYBR Green I dye,

fluorescein passive reference dye, and dUTP for optional carryover contamination control. After thawing and mixing, the required components were added to make a reaction master mix for each 25 μL reaction. Template DNA (≤ 100 ng/reaction) was added, and the thermal cycler was programmed for an initial heating step of 95°C for 10 minutes, followed by 45 cycles of 95°C for 10 seconds, 60°C for 15 seconds, and 72°C for 15 seconds. Melting curve analysis was performed between 72°C and 95°C at a rate of 1°C per second.

One microgram of total RNA was converted into single-stranded complementary DNA (cDNA) using the QuantiTect Reverse Transcription Kit (Qiagen, USA). The gDNA Wipeout solution was used to remove genomic DNA. Random hexamers served as primers. Amplification began with 30 ng of total cDNA and ended with 300 nM of each primer pair (Table 1). Each sample underwent triplicate real-time PCR, and the average results were used for further analysis. Ubiquitin 5 (UBQ5) served as the reference gene. Data were generated automatically based on threshold Cycle (Ct) values. The ΔCt values for each sample were calculated by adjusting to the average Ct value of the reference genes.

Following Livak and Schmittgen²³, the relative expression of the target gene was determined using the $2^{-\Delta\Delta\text{Ct}}$ method. The control group served as the calibrator, and the other dietary groups served as experiments. The fold change was calculated as $(2^{-\Delta\Delta\text{Ct}})$.

Detection of cytokines

Commercially available kits from R&D Systems, USA, were used to quantify the levels of cytokines in rat blood, including Interleukin-6 (IL-6), Interleukin-1 beta (IL-1 β), and Tumor Necrosis Factor-alpha (TNF- α). The manufacturer's instructions were followed precisely. The standard cytokine curve was on the same sample plate as the measured cytokine concentrations.

Immunohistochemistry for BAX and BCL2

Rat brain tissue was either freshly collected or obtained from a previously fixed specimen. For fresh tissue, brains were immersed in 4% paraformaldehyde in phosphate-buffered saline (PBS) for 4 hours at 4°C . For frozen sections, tissues were fixed in 4% paraformaldehyde overnight, then cryoprotected in 30% sucrose in PBS until they sank, typically overnight at 4°C . The tissue was embedded in OCT compound, frozen using liquid nitrogen, and sectioned (10–20 μm thick) using a cryostat. Sections were mounted onto glass slides.

Table 1: Primer primers for genes under study

Genes	Primers	References
<i>AChE</i>	5'-AAT CGA GTT CAT CTT TGG GCT CCC CC-3'	Xia et al. 2022
	5'-CCA GTG CAC CAT GTA GGA GCT CCA-3'	
<i>GAPDH</i>	5'-AAC GGA TTT GGC CGT ATT GG-3'	Xia et al. 2022
	5'-CTT CCC GTT CAG CTC TGG G-3'	
<i>MAO-A</i>	5'-GCCAAGATTCACTTCAGACCAGAG-3'	Alkhalwaldeh and Bardaweel, 2023
	5'-TGCTCCTCACACCAGTTCTTCTC-3'	

Sections were incubated in blocking solution containing 5% bovine serum albumin (BSA) in PBS for 1 hour at room temperature to prevent non-specific binding and then treated with 0.1% Triton X-100 in PBS for 15 minutes at room temperature for permeabilization. Antigen retrieval was performed by heating sections in citrate buffer (pH 6.0) at 95°C for 20 minutes, followed by cooling and washing. Sections were incubated overnight at 4°C with primary antibodies against Bax (Rabbit anti-Bax, diluted 1:200) and Bcl-2 (Rabbit anti-Bcl-2, diluted 1:200).

After washing three times with PBS, the sections were incubated with appropriate secondary antibodies conjugated to fluorophores for 1–2 hours at room temperature in the dark. The sections were washed again, and nuclei were counterstained with DAPI (1 µg/mL) for 5 minutes. Finally, the sections were mounted in an anti-fade medium and examined under a fluorescence microscope. Images were captured with filters corresponding to the specific fluorophores, and Bax and Bcl-2 expression patterns were analyzed both qualitatively and quantitatively.

Oxidative Stress Parameters

Malondialdehyde (MDA) levels (a marker of lipid peroxidation indicating oxidative injury), superoxide dismutase (SOD) activity (a key antioxidant enzyme), reduced glutathione (GSH) levels (a major cellular antioxidant), catalase activity (an antioxidant enzyme critical for hydrogen peroxide clearance), and nuclear factor Kappa-B (NFκB) (the key transcriptional regulator of the inflammatory pathway) will be determined in the brain tissues.

Western blot analysis will be employed to assess the expression levels of apoptosis markers (cleaved caspase-3) and neurotrophic factors (brain-derived neurotrophic factor, BDNF). In addition, amyloid precursor protein (APP) levels will be analyzed by western blotting.

Histopathological analysis

We preserved skeletal muscle tissue samples in 10% formal saline, then sectioned, cleaned, and dehydrated them in increasing concentrations of alcohol. We cleared the dehydrated specimens in xylene, fixed them in paraffin blocks, and sectioned them to a thickness of 4–6 µm. We removed the paraffin from the tissue slices using xylene and then stained them with hematoxylin and eosin (H&E). An electric light microscope was used for histopathological analysis²⁴.

Statistical analysis

The sample size for this study was determined according to the 3Rs ethical principles (replacement, reduction, and refinement) in animal research. A post hoc power analysis was conducted using G*Power (version 3.1.9.7) to assess the sufficiency of the sample size²⁵. Based on an effect size ($d = 0.7$), an alpha level (α) of 0.05, 80% power, and type II error, the analysis indicated that a total sample size of 32 rats (8 rats per group) was sufficient for detecting statistically significant differences. Values for all parameters are presented as the mean \pm SEM. To determine if there were statistically significant differences among the groups, we used SPSS 23.0 and a one-way analysis of variance (ANOVA) followed by Tukey's multiple comparison tests. We considered findings significant if $p < 0.05$.

RESULTS

FTIR analysis

We used Fourier transform infrared spectroscopy (FTIR) to identify the functional groups of arabinogalactans isolated from the scaffolds (Figure 1a). The FTIR spectrum revealed several absorption bands indicating different functional groups. The broadening of the 3242.40 cm^{-1} peak indicates O-H broadening vibrations, which are associated with hydroxyl groups. Phenolic compounds and polysaccharides commonly contain these groups. The peak at 2921.27

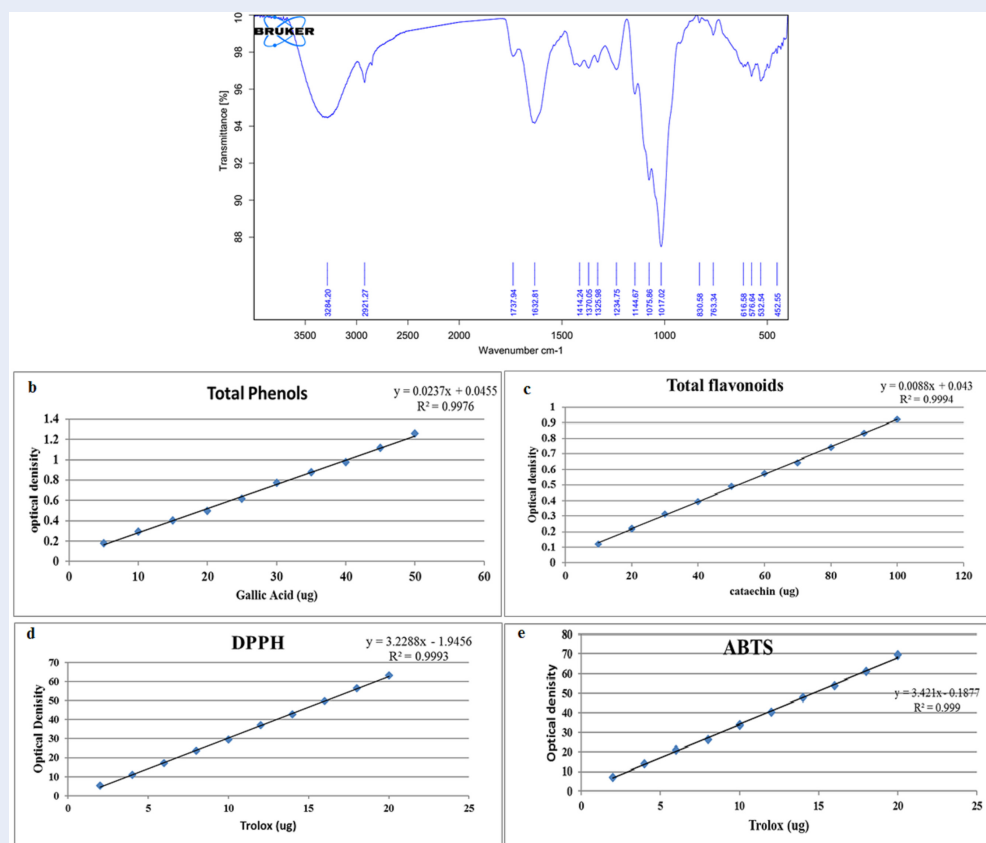


Figure 1: Characterization of MAG extract. **a**) Attenuated Total Reflectance – Fourier Transform Infrared Spectroscopy (ATR-FTIR) spectrum of MAG, illustrating key peaks corresponding to functional groups, including O-H (3284 cm^{-1}), C-H (2921 cm^{-1}), C=O (1737 cm^{-1}), and C-O-C (1075 cm^{-1}), confirming the polysaccharide and phenolic composition of the extract, **b**) Standard calibration curve for total phenolic content using Gallic acid as a reference, showing a linear relationship between absorbance and concentration ($R^2 > 0.99$), **c**) Standard calibration curve for total flavonoid content using catechin as a reference, demonstrating a linear correlation ($R^2 > 0.99$), **d**) DPPH radical scavenging assay calibration curve using Trolox as a standard ($R^2 > 0.99$), quantifying antioxidant capacity, **e**) ABTS assay calibration curve using Trolox as a reference ($R^2 > 0.99$), illustrating the extract's antioxidant potential.

cm^{-1} coincides with C-H stretching vibrations, indicating the presence of aliphatic chains in the extract. The peak at 1739.94 cm^{-1} is caused by C=O stretching vibrations, which are common in carbonyl groups such as esters or carboxylic acids. The band at 1638.21 cm^{-1} is caused by C=C stretching vibrations, which are likely related to the aromatic ring of phenolic compounds. Moreover, there is a broad peak around $3300\text{--}3500\text{ cm}^{-1}$, which could correspond to O-H stretching (typical for gallic acid) or N-H stretching (typical for melatonin). There is a strong peak around 1700 cm^{-1} (specifically at 1713 cm^{-1}), which could be the C=O stretching of carboxylic acid in gallic acid or the amide C=O in melatonin. The 1414.24 cm^{-1} peak corresponds to C-H bending vibrations, common in various organic compounds. The band

at 1243.67 cm^{-1} suggests the presence of ether or ester functional groups (C-O propagation vibration). The distinguishing characteristics of glycosidic bonds in polysaccharides, which manifest as a strong band at 1078.56 cm^{-1} , are the C-O-C propagation vibrations (1017.02 cm^{-1} , 880.95 cm^{-1} , 779.34 cm^{-1} , 616.59 cm^{-1} , 579.45 cm^{-1}).

Total phenolic, flavonoid contents, and antioxidants

The total phenolic content of the extract was found to be $341.74\text{ }\mu\text{g GAE/g}$ (Figure 1 b). This indicates a high content of phenolic compounds known to have antioxidant properties. We also measured the total flavonoid content, which was $95.00\text{ }\mu\text{g CE/g}$. Flavonoids are important for preventing oxidative

stress. The total flavonoid content was determined by means of a calibration curve prepared with catechins (Figure 1c) and expressed as micrograms of catechin equivalent ($\mu\text{g CE}$) per g. In our study, we tested the antioxidant properties of arabinogalactans extract using two different assays: DPPH and ABTS. The DPPH assay (Figure 1d) showed an antioxidant activity of $317.43 \mu\text{g TE/g}$, while the ABTS assay showed a slightly higher activity of $352.96 \mu\text{g TE/g}$. These results indicate that the scaffold has strong antioxidant properties for the production of arabinogalactans water from it. If the observed absorbance value exceeded the linear range of the standard curve, further dilution was performed. The ABTS standard curve was generated utilizing Trolox (Figure 1e). Results were presented as $\mu\text{g Trolox equivalents (TE)}$ per gram.

Western blotting findings BDNF, cleaved caspase-3

Under different treatment settings, the expression levels of the Brain-Derived Neurotrophic Factor (BDNF) antibody were analyzed (Figure 2). The control group exhibited a BDNF expression level of 46.01%, serving as the baseline for comparison. Exposure to radiation significantly decreased BDNF expression, with a lane percentage of 14.88%. This reduction highlights the detrimental effect of radiation on BDNF levels. After radiation exposure and MAG treatment, rats exhibited a BDNF expression level of 30.37%.

The expression levels of anti-cleaved caspase-3 were assessed in control and treated rat samples, with findings displayed as lane percentages (Figure 3). The control group had expression levels of 10.83% and 39.46%. The group exposed to radiation had significantly reduced expression levels of 9.37% and 15.73%. Finally, the cohort that had a particular therapy (MAG) exhibited expression levels of 10.69% and 27.69%. This indicates a potential protective role of antioxidants against radiation-induced cellular damage, as observed in the treated sample group with intermediate expression levels.

QPCR Analysis for AChE, NF- κ B, and MAO-A

The expression levels of the *AChE*, *NF- κ B*, and *MAO-A* genes were analyzed using the double delta Ct ($\Delta\Delta\text{Ct}$) method (Figure 4). Four experimental conditions were examined: Control, Antioxidant treatment, Radiation exposure, and a combined Treatment group. The housekeeping gene used for normalization was GAPDH (Table 1).

The control group served as the reference, hence a 1.0-fold change. This established the basal expression level of the *AChE* gene. No change in the expression was observed for the *AChE* gene against the control group (a fold change of 1.0), which suggests that antioxidant treatment does not strongly influence *AChE* gene expression. Radiation exposure strongly reduced the expression of the *AChE* gene, with a fold change decrease to 0.5. This strong reduction may indicate that radiation exposure inhibited *AChE* gene expression, possibly due to stress-induced changes in gene regulation. The treatment group (MAG) exhibited a fold change of 0.7, indicating a downregulation of *AChE* gene expression compared to the control, but less severe than that observed with radiation exposure alone.

In the treatment group, the fold change in the expression of *MAO-A* was 1.4, indicating this gene was elevated compared with the control, but less than the elevation following radiation alone.

Markers of Oxidative Stress in the Brain

The results of the effect of the administration of Matcha Arabinogalactans on markers of oxidative stress before and after radiation exposure are summarized in Table 2.

The levels of MDA, indicative of lipid peroxidation and oxidative damage, were markedly elevated in the radiation-exposed groups compared to the control group ($4.00 \pm 0.05 \text{ nmol/mg protein}$ vs. $1.20 \pm 0.005 \text{ nmol/mg protein}$). In the cohort of MAG (B & A- γ rays) therapy, MDA levels were markedly decreased compared to the radiation-only group ($2.20 \pm 0.05 \text{ nmol/mg protein}$, $F(3, 28) = 1633.90$, $P < 0.001$).

The activity of superoxide dismutase (SOD), a crucial antioxidant enzyme, was markedly reduced in the radiation-exposed group relative to the control group ($3.01 \pm 0.05 \text{ U/mg protein}$ vs. $5.18 \pm 0.05 \text{ U/mg protein}$, respectively). In the group treated with MGA (B & A- γ rays), SOD activity was significantly higher compared to the radiation-only group ($4.23 \pm 0.04 \text{ U/mg protein}$, $F(3, 28) = 501.41$, $P < 0.001$), demonstrating the potential of MAG to mitigate radiation-induced oxidative stress.

When comparing the radiation group to the control group, there was a substantial decrease in GSH levels ($4.36 \pm 0.30 \mu\text{mol/g tissue}$ vs. $12.94 \pm 0.06 \mu\text{mol/g tissue}$, respectively), which is the main cellular antioxidant. In the MGA + γ -rays + MAG group, GSH levels were significantly higher compared to the radiation-only group ($10.31 \pm 0.28 \mu\text{mol/g tissue}$, $F(3, 28) = 377.56$, $P < 0.001$), indicating the restorative effect of MAG on GSH levels following radiation exposure.

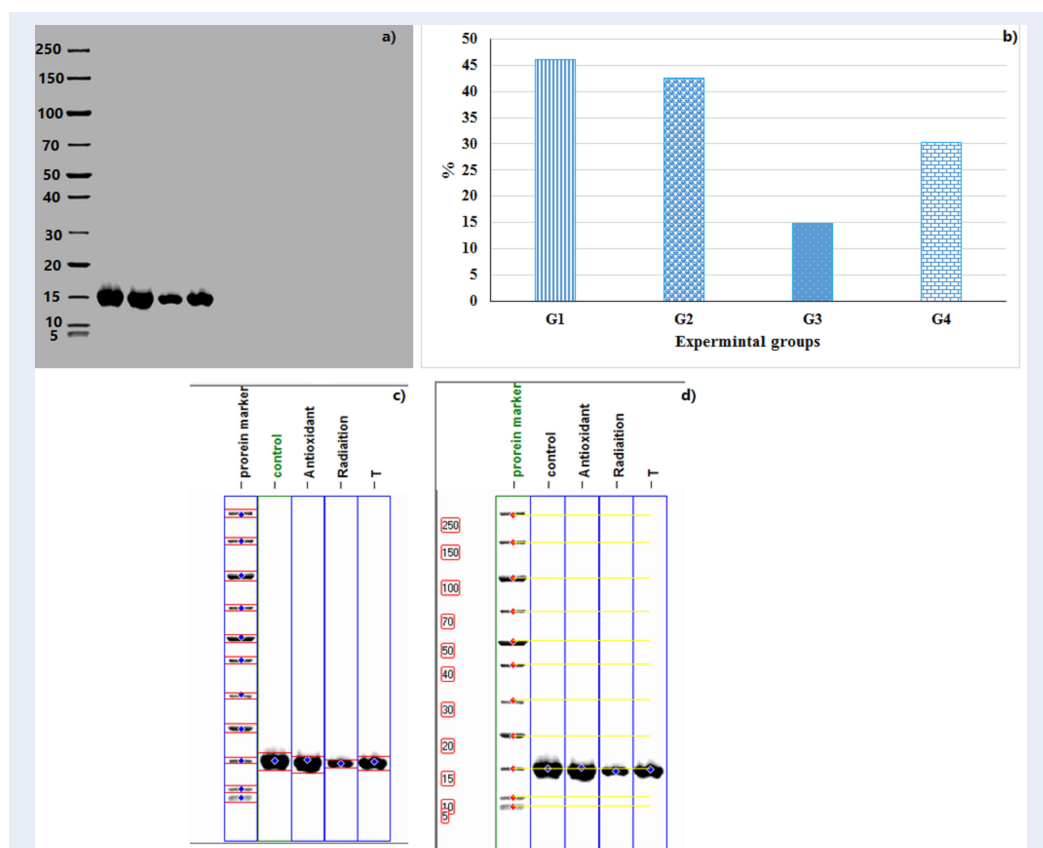


Figure 2: The Brain-Derived Neurotrophic Factor (BDNF) before and after treatments. a) Western blot of BDNF expression, with molecular weight markers (250–10 kDa) shown on the left. β -actin (~42 kDa) was used as a loading control for normalization, b) Computerized analysis of Brain-Derived Neurotrophic Factor (BDNF) antibody protein expression level for samples, c) Densitometric analysis of BDNF expression across experimental groups under different conditions, showing anti- Brain-Derived Neurotrophic Factor (BDNF) band calculation for samples, d) A similar densitometric analysis to panel c, showing BDNF expression under slightly different experimental conditions. The molecular weight markers are indicated on the left, while the relative expression levels of BDNF are plotted in the treatment lanes.

Table 2: Effect of MAG before and after treatments on oxidative stress in rats

Treatment Group	Control	MAG	Rad	MAG+ Rad	F-value	P-value
MDA (nmol/mg)	1.20±0.005c	1.14±0.005c	4.00±0.05a	2.20±0.05b	1633.90*	<0.001
SOD (U/mg protein)	5.18±0.05b	5.36±0.05a	3.01±0.05d	4.23±0.04c	501.41*	<0.001
GSH (μ mol/g tissue)	12.94±0.06a	13.10±0.07a	4.36±0.30c	10.31±0.28b	377.56*	<0.001
CAT (U/mg protein)	48.13±0.10a	48.95±0.09a	34.49±0.18c	40.23±0.39b	944.19	<0.001

Results are presented as the mean \pm SE, n= 8. One-way ANOVA followed by Tukey’s post hoc test was performed. The groups are statistically significant (p<0.05) as compared with control. The same superscript in the same raw are not statistically different.

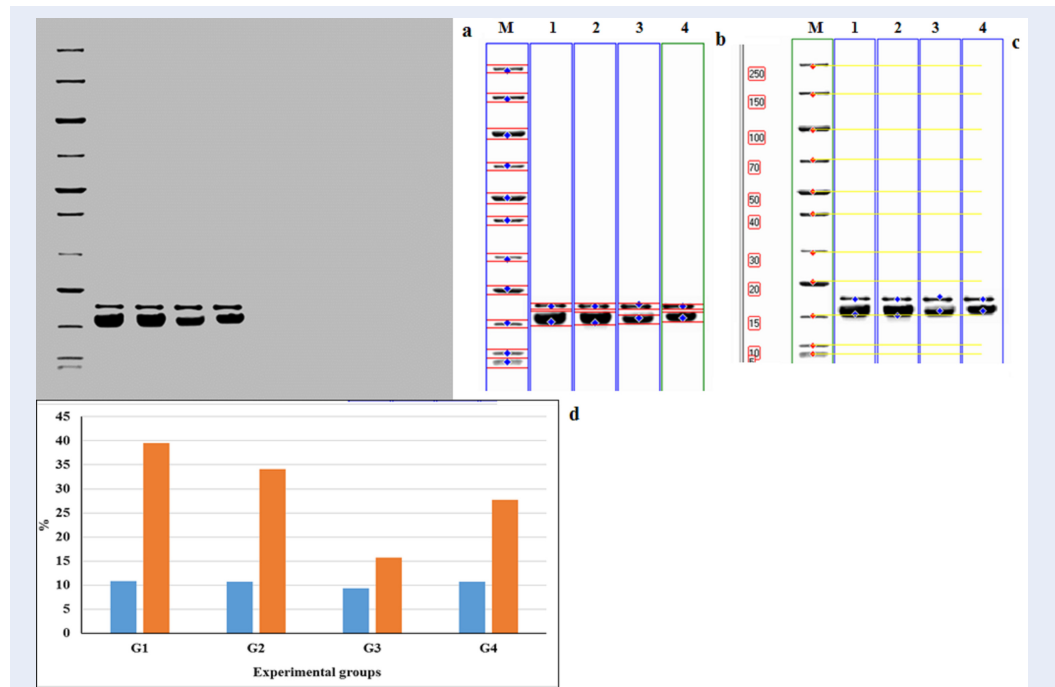


Figure 3: Analysis of cleaved caspase-3 expression via Western blot. a) Western blot of cleaved caspase-3 expression, with molecular weight markers shown on the left. β -actin served as the normalization control. The molecular weight marker (M) is shown on the left, and lanes 1 to 4 represent different experimental conditions, with protein bands corresponding to cleaved caspase-3. The molecular weight marker confirmed cleaved caspase-3 detection at ~17 kDa, b) Computerized analysis of cleaved caspase-3 expression across experimental groups, with lanes labeled for each condition. The protein marker on the left indicates molecular weights ranging from 250 kDa to 10 kDa, c) Anti-cleaved caspase-3 band calculation for samples, d) Bar graph representation of the relative percentage of cleaved caspase-3 expression in four experimental groups (G1, G2, G3, and G4).

CAT activity, vital for hydrogen peroxide clearance, was significantly lower in the radiation-exposed group compared to the control group (34.49 ± 0.18 U/mg protein vs. 48.13 ± 0.10 U/mg protein, respectively). Treatment with MAG (B & A- γ rays) significantly improved CAT activity compared to the radiation-only group (40.23 ± 0.39 U/mg protein, $F(3, 28) = 944.19$, $p < 0.001$), highlighting the potential of MAG in enhancing antioxidant defenses against radiation-induced oxidative stress.

Cytokines TNF- α , IL-1 β , and IL-6 levels

The study results show significant changes in different cytokines across the various treatment groups (Table 3). TNF- α levels were significantly higher in the Rad group (25.75 ± 0.34 pg/ml) than in the control (12.20 ± 0.35 pg/ml). In the MGA (B & A- γ rays) group, TNF- α was 16.61 ± 0.20 , $F(3, 28) = 525.74$, $p < 0.001$.

Similarly, IL-1 β levels were the highest in the Rad group (18.32 ± 0.31 pg/ml) compared to the control (8.31 ± 0.26 pg/ml). Treatment with MAG (B & A- γ

rays) reduced IL-1 β to 12.51 ± 0.19 pg/ml, $F(3, 28) = 405.21$, $p < 0.001$.

IL-6 levels followed a similar trend, showing the highest levels in the Rad group (28.40 ± 0.33), compared to the control (14.58 ± 0.18). In the MAG (B & A- γ rays) group, IL-6 was 19.89 ± 0.28 , $F(3, 28) = 752.89$, $p < 0.001$.

Immunohistochemistry for BAX

The control group showed weak BAX expression in the neurons of brain tissue, and a similar result was detected in the antioxidant group. Conversely, a significantly higher increase in BAX expression was observed in the gamma rays group compared to the other experimental groups (Figure 5).

Immunohistochemistry for Bcl2

The control group showed weak Bcl2 expression in the neurons of brain tissue, and a similar result was detected in the antioxidant group. Conversely, a significant decrease in Bcl2 expression was observed in the

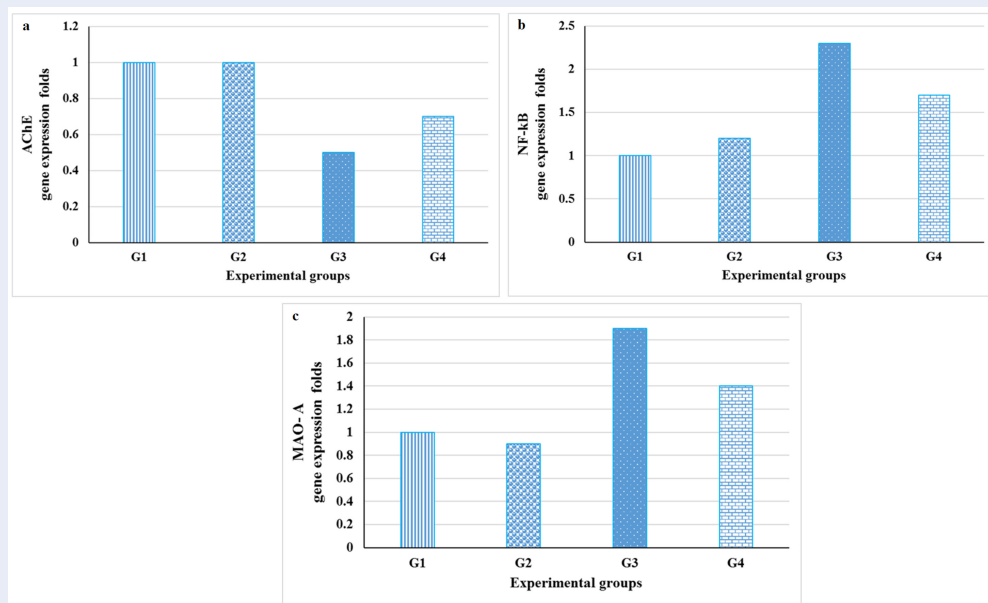


Figure 4: QPCR results using the Double Delta Ct method, which is commonly employed for relative quantification of gene expression levels. a) Bar graph showing the relative expression levels of the acetylcholinesterase (AChE) gene across four experimental groups (G1, G2, G3, and G4). **b)** The expression levels of the NF-κB (Nuclear Factor kappa-light-chain-enhancer of activated B cells) gene across the same experimental groups, **c)** Bar graph representing the expression levels of the monoamine oxidase A (MAO-A) gene across the four experimental groups.

Table 3: Effect of MAG before and after treatments on cytokines in rats

Treatment Group	Control	MAG	Rad	MAG+ Rad	F-value	P-value
TNF-α (pg/ml)	12.20±0.35 ^c	11.86±0.18 ^c	25.75±0.34 ^a	16.61±0.20 ^b	525.74*	<0.001
IL1β (pg/ml)	8.31±0.26 ^c	8.14±0.18 ^c	18.32±0.31 ^a	12.51±0.19 ^b	405.21*	<0.001
IL-6 (pg/ml)	14.58±0.18 ^c	14.19±0.10 ^c	28.40±0.33 ^a	19.89±0.28 ^b	752.89*	<0.001

Results are presented as the mean ± SE, n = 8. One-way ANOVA followed by Tukey’s post hoc test was performed. The groups are statistically significant (p < 0.05) as compared with control. The same superscript in the same raw are not statistically different.

gamma rays group compared to the other experimental groups (Figure 6).

Lesions were scored based on the severity of the histological changes observed. Brain tissue in the control group was healthy and intact, with no signs of damage or abnormality. The lesion score of this group was 0, indicating no histopathological lesions (Figure 7a). Similarly, brain tissue from the antibiotic-treated control group showed cerebral atrophy, but muscle and nerve cells were unaffected and maintained their normal structure. The lesion score was 0, indicating no lesion (Figure 7b).

In contrast, the brain tissue of the gamma radiation group showed more damage. The parenchyma exhibited obvious blood vessels (indicated by arrows) and numerous empty vessels (indicated by arrows). These

histopathological changes resulted in a ++ lesion score, indicative of severe brain damage (Figure 7c). Brain tissue from the group exposed to both gamma radiation and antibiotics showed significant improvement compared to the gamma ray-only group, with an absence of parenchyma blood vessels and tissue formation only weakly in muscle cells (indicated by arrows). This group had a lesion score of +, indicating a significant reduction in neurologic damage (Figure 7d).

DISCUSSION

The results of this study demonstrated that the extracted compounds exhibit structural and functional features consistent with polysaccharides, specifically arabinogalactans. Both Fourier Transform Infrared

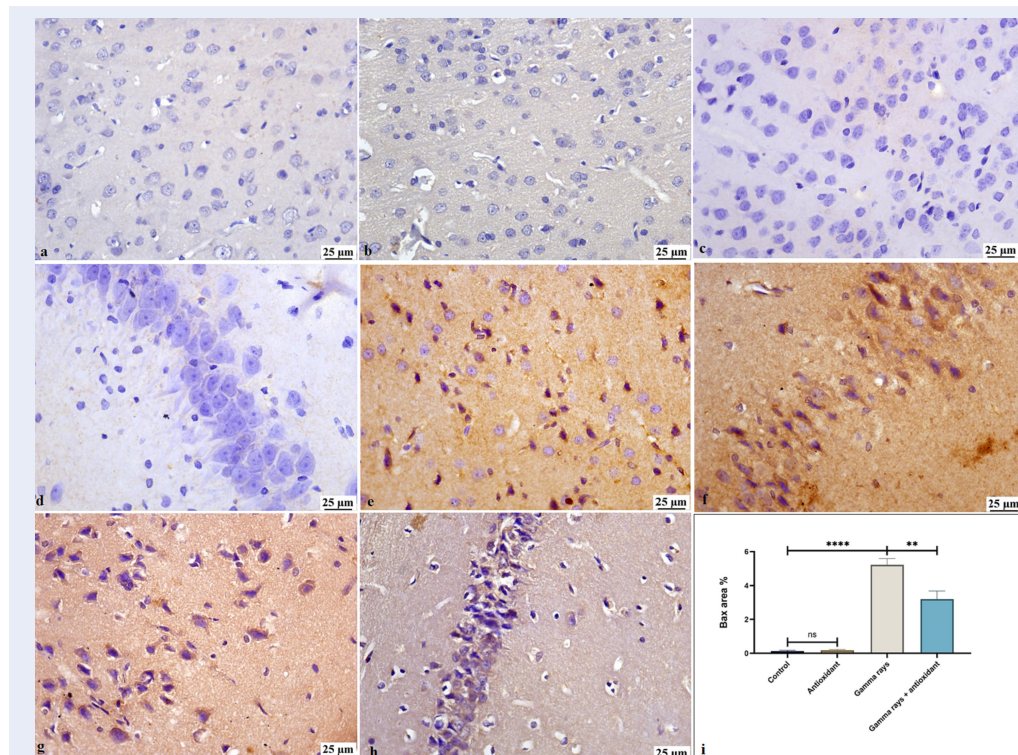


Figure 5: Immunohistochemistry analysis for Bax protein expression in the brain of rats before and after MAG treatment, using a magnification scale of 25 μm to assess apoptotic activity in the different experimental groups. a) Control group showing baseline expression levels of Bax in the brain tissue, with sparse Bax-positive cells, b) Photomicrograph of brain, control group showing weak Bax expression in the cerebral cortex, c) The cerebral cortex in normal rats were received MGA, d) the hippocampus in normal rats were received MGA, e) Photomicrograph of brain, gamma rays group showing higher Bax expression in the cerebral, f) The hippocampus, gamma rays group showing higher Bax expression, g) Photomicrograph of brain, gamma rays + MGA group showing moderate Bax expression in the hippocampus (Immune staining), h) Chart represents Bax expression as mean area percent of positive staining. Data are presented as mean \pm SE. Significant difference is considered at $P < 0.05$.

(FTIR) spectroscopy and High-Performance Liquid Chromatography (HPLC) analyses provided complementary insights into the chemical composition and bioactive potential of the extract.

FTIR spectra revealed key functional groups indicative of polysaccharides. Peaks observed at 3284 cm^{-1} correspond to O-H stretching vibrations, characteristic of hydroxyl groups typically present in polysaccharides like arabinogalactans²⁶. The peak at 1075 cm^{-1} , attributed to C-O-C stretching, confirms the presence of glycosidic linkages, which are a hallmark of polysaccharide structures^{27,28}. The C=O stretching observed at 1737 cm^{-1} and C-H stretching at 2921 cm^{-1} further support the presence of aliphatic and carbonyl functional groups in the extract²⁹⁻³¹. Additionally, Wu *et al.*³² emphasized the utility of FTIR in detecting glycosidic bonds and hydroxyl groups in arabinogalactans, providing further validation of the

results.

HPLC analysis provided quantitative data on the bioactive components of the extract. Notably, phenolic compounds such as Gallic acid and Chlorogenic acid were identified. These compounds are known for their antioxidant properties, which contribute to the therapeutic potential of arabinogalactan-containing extracts³³. The presence of these compounds suggests that the extract is not only polysaccharide-rich but also enriched with bioactive phenolics, which may enhance its functional properties.

The retention times and peak areas obtained in this study are consistent with those reported by Saeidy *et al.*¹, who quantified bioactive components in polysaccharide extracts using HPLC. These results further corroborate the structural and functional identity of the extract.

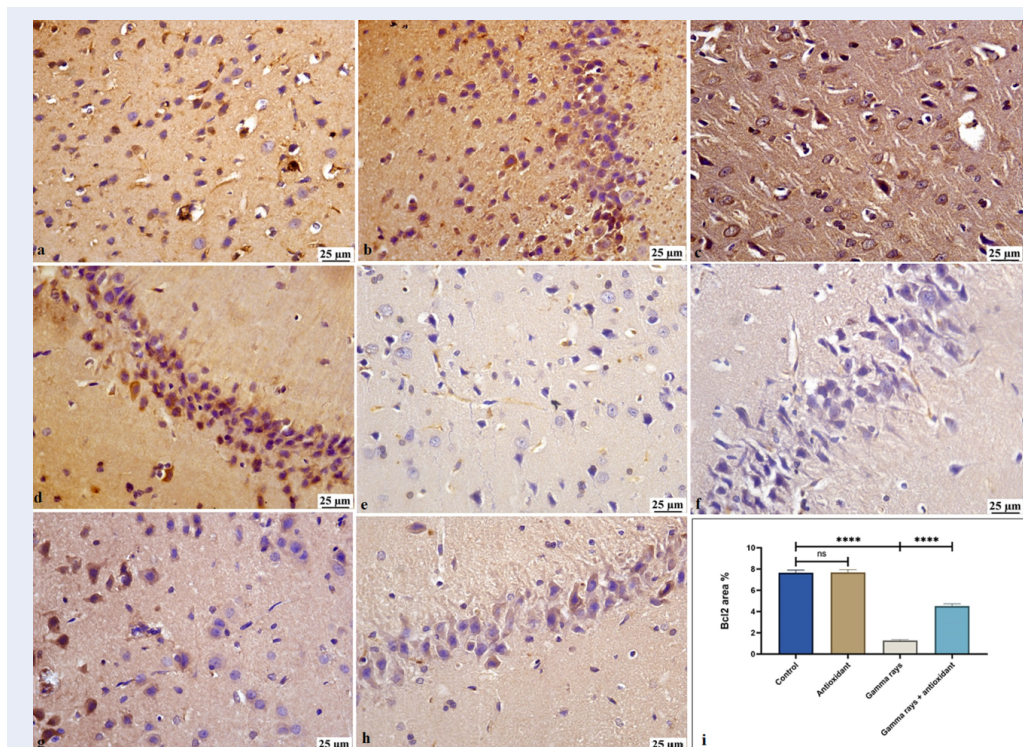


Figure 6: Immunohistochemistry for bcl2 before and after treatments. **a)** Photomicrograph of brain, control group showing higher Bcl2 expression in the cerebral cortex (Immune staining), **b)** Photomicrograph of brain, control group showing higher Bcl2 expression in the hippocampus (Immune staining), **c)** Photomicrograph of brain, MGA group showing higher Bcl2 expression in the cerebral cortex (Immune staining), **d)** Photomicrograph of brain, MGA group showing higher Bcl2 expression in the hippocampus (Immune staining), **e)** Photomicrograph of brain, gamma rays group showing lower Bcl2 expression in the cerebral cortex (Immune staining), **f)** Photomicrograph of brain, gamma rays group showing lower Bcl2 expression in the hippocampus (Immune staining), **g)** Photomicrograph of brain, gamma rays + MGA (B& A) group showing moderate Bcl2 expression in the cerebral cortex (Immune staining), **h)** Photomicrograph of brain, gamma rays + antioxidant group showing moderate Bcl2 expression in the hippocampus (Immune staining), **i)** Chart represents Bcl2 expression as mean area percent of positive staining. Data are presented as mean \pm SE. Significant difference is considered at $P < 0.05$.

The presence of glycosidic linkages and hydroxyl groups, as confirmed by FTIR, strongly supports the hypothesis that the extract contains arabinogalactans. Arabinogalactans are known for their immunomodulatory, antioxidant, and anti-inflammatory properties, as highlighted by Wang *et al.*³⁴. Furthermore, the detection of phenolic compounds via HPLC suggests a synergistic contribution to the extract's antioxidant activity^{35,36}. Baumann *et al.*⁹ identified similar glycosidic structures in arabinogalactans that contribute to their bioactivity, supporting our FTIR findings of polysaccharide-rich MAG with glycosidic linkages. The data clearly demonstrate that radiation exposure significantly decreases the expression of BDNF, aligning with earlier research that indicates a harmful effect of radiation on neurological well-being^{37,38}. The partial recovery of BDNF levels in the treatment group, however, suggests that the provision of antioxidants

lessens this impact. These data corroborate the concept that antioxidants might confer neuroprotective advantages in the setting of radiation exposure.

The expression of anti-cleaved caspase-3 in controls and treated samples may present important information on the responses of cells to different therapies. Anti-cleaved caspase-3 is an apoptosis biomarker. The degree of programmed cell death under diverse situations is reflected by its expression levels³⁹.

The baseline expression levels of 10.83% and 39.46% in the control group serve as a reference for normal physiological circumstances in rats. The group treated with antioxidants exhibited a modest decrease in anti-cleaved caspase-3 expression (10.71% and 34.12%), indicating that antioxidants may mitigate apoptosis under normal circumstances.

Radiation exposure significantly reduced anti-cleaved caspase-3 expression levels to 9.37% and 15.73%, re-

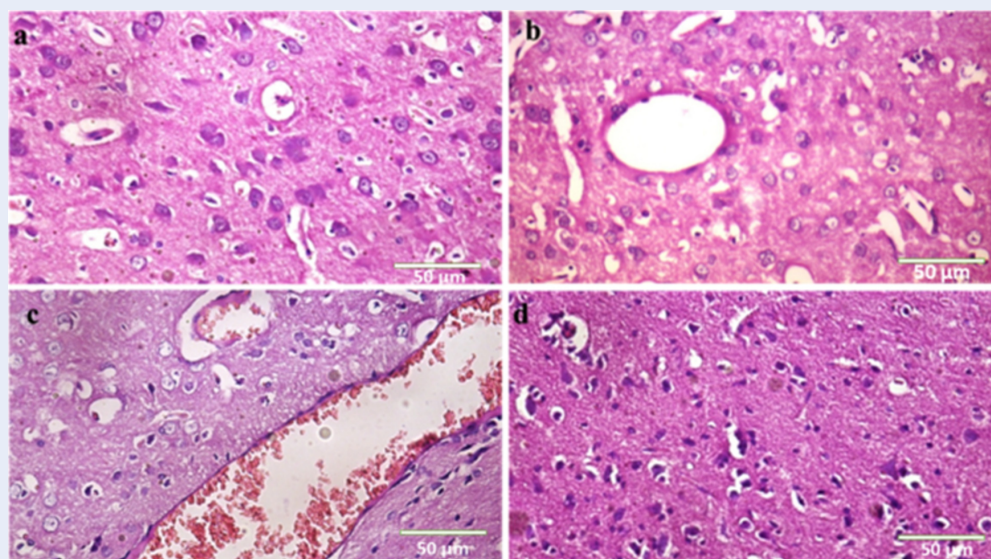


Figure 7: Histopathological of brain. **a)** Brain from control normal group showing normal brain parenchyma; notice the normal neurons and nerve cells, (Lesion score: 0), (Scale bare 50 μm), **b)** Brain from control normal + Antioxidant group showing normal brain parenchyma; notice the normal neurons and nerve cells, (Lesion score: 0), (Scale bare 50 μm), **c)** Brain from Gamma rays exposed group showing damaged brain parenchyma; notice the blood vessel congestion (arrow head) and vacuolated nerve cells (arrows), (Lesion score: ++), (Scale bare 50 μm), **d)** Brain from Gamma rays + Antioxidant exposed group showing marked improved brain parenchyma; notice the absence of blood vessel congestion with mild vacuolated nerve cells (arrows), (Lesion score: +), (Scale bare 50 μm).

spectively. This substantial decrease indicates that radiation induces a strong apoptotic response, leading to increased cell death⁴⁰. The diminished expression of anti-cleaved caspase-3 may arise from significant cellular damage and the onset of apoptosis, ultimately culminating in caspase-3 cleavage and activation. The group administered both antioxidants and an additional modality (perhaps a combined therapy including radiation) had intermediate expression levels of 10.69% and 27.69%. The findings indicate that while radiation necrosis occurs, antioxidants can mitigate cellular damage and apoptosis to some extent. These medicines help eliminate microorganisms that exacerbate radiation-induced damage, thereby mitigating the adverse effects of radiation therapy. Future medicine highlights the advantages⁴¹.

The reported results align with the idea that antioxidants might mitigate oxidative stress and decrease apoptosis. The protective function of this antioxidant against radiation-induced damage underscores its potential therapeutic advantages in reducing adverse effects in clinical radiation treatment settings.

The results found align with the idea that antioxidants might mitigate oxidative stress and decrease apoptosis. The reduction in anti-cleaved caspase-3 expression in the antioxidant-treated group substantiates the

notion that antioxidants contribute to cellular health and functionality. Furthermore, the intermediate expression levels in the combined therapy group indicate that antioxidants provide a degree of protection; however, they are unable to fully mitigate the effects of radiation⁴².

The expression levels of anti-cleaved caspase-3, a significant apoptosis marker, were examined in control and treated rat tissues to elucidate cellular responses to various treatments. Our findings provide substantial insights into the possible protective effects of antioxidants against radiation-induced apoptosis⁴³.

The expression levels in the base state were 10.83% and 39.46% for the control group, representing a normal physiological state, which served as a background against which later stages were compared. Antioxidant treatment only marginally reduced the levels of expression to 10.71% and 34.12%, respectively; this represents minimal influence on the basal apoptotic rates under normal conditions. A finding of this nature could suggest that antioxidants preserved cellular integrity by not significantly interfering with normal cell mechanisms that lead to apoptosis.

Radiation exposure significantly down-regulated anti-cleaved caspase-3 expression to 9.37% and

15.73%, respectively, demonstrating a great increase in apoptotic activity. The pronounced reduction underlines the pro-apoptotic effect of radiation, most likely as part of severe cellular stress and damage that eventually leads to the induction of caspase pathways. The cohort subjected to a combination regimen of antioxidants and radiation had intermediate expression levels of 10.69% and 27.69%. These levels exceed those recorded with radiation alone but are lower than those of the control and antioxidant-only groups. This indicates that antioxidants provide a limited protective effect against radiation-induced apoptosis. The moderate expression levels suggest that although antioxidants cannot entirely negate the effects of radiation, they substantially reduce the degree of apoptosis, thereby providing some cellular protection.

These findings corroborate other research indicating the protective function of antioxidants against oxidative stress and apoptosis. The capacity of antioxidants to diminish apoptotic markers in the context of radiation highlights their prospective therapeutic utility in clinical scenarios involving unavoidable radiation exposure, such as cancer treatment⁴⁴.

These results are important because they ensure that the dual role of radiation in inducing apoptosis, as well as the capacity of antioxidants to modulate this response, is emphasized. The decreased anti-cleaved caspase-3 expression noted in the combined therapy group supports the synergistic role of antioxidants in mitigating the adverse effects of radiation. The inadequacy of antioxidants to fully neutralize radiation effects underscores the necessity for improving dose and combination techniques to achieve better protective outcomes.

These data show that both radiation exposure and combination therapy have a profound impact on MAO-A gene expression, while antioxidant treatment alone only minimally affects it. The increase induced by radiation underlines the sensitivity of MAO-A expression to environmental stresses. The findings contribute to our knowledge of the molecular processes underlying stress responses and on the eventual therapeutic benefits of antioxidants.

The differential expression identified here highlights the importance of considering environmental and treatment variables in studies concerned with gene regulation. Further study will be required to explain the specific mechanisms of these therapies on the expression of the MAO-A gene and further elucidate the regulation of this important gene with respect to stress and therapeutic interventional approaches.

TNF- α , IL-1 β , and IL-6 are important cytokines implicated in inflammatory and immune reactions.

These cytokines were significantly influenced by MGA before and after irradiation, with remarkable reductions in the levels of TNF- α , IL-1 β , and IL-6. This suggests a possible immunomodulatory impact of MGA. Our findings indicate that radiation markedly raises the levels of TNF- α , IL-1 β , and IL-6, but MGA therapy seems to alleviate these radiation-induced elevations.

The increase in pro-inflammatory cytokines after radiation exposure aligns with prior research. Najafi *et al.*⁴⁵ indicated elevated levels of TNF- α and IL-6 in irradiated tissues, indicating that these cytokines are integral to radiation-induced inflammatory responses. Wei *et al.*⁴⁶ similarly discovered that radiation exposure resulted in elevated IL-1 β production across several organs, hence contributing to both acute and chronic inflammation.

The protective effect of MGA in our model is in agreement with the well-documented anti-inflammatory and antioxidant properties of melatonin and gallic acid. In fact, it has been reported that melatonin may control the expression of proinflammatory cytokines in various experimental models. Gallic acid has been mentioned to inhibit NF- κ B activation—one of the main transcription factors controlling the inflammatory process—thus decreasing the expression levels of proinflammatory cytokines⁴⁷.

These observations might indicate that the combined action of melatonin and gallic acid in our MGA therapy is responsible for its potency in mitigating radiation-induced inflammation. Since the levels of pro-inflammatory cytokines were intermediate in the MGA + Rad group compared to the Rad group, this combination has the potential to have a considerably stronger preventive impact than either drug alone.

Our findings include significant implications for radiation protection and therapy. MGA's capacity to reduce radiation-induced elevations in pro-inflammatory cytokines indicates its promise as a radioprotective agent. This may be especially beneficial in radiation treatment contexts, where minimizing collateral damage to healthy tissues is a significant concern^{47,48}.

The findings indicate that radiation exposure markedly elevates oxidative stress in rat brain tissues, as seen by increased MDA levels and diminished activity of essential antioxidant enzymes (SOD, GSH, and CAT). Treatment with Matcha Arabinogalactans (MAG) demonstrates protective potential, decreasing oxidative damage and bolstering antioxidant defenses. This points to the fact that MAG acts protectively against radiation-induced oxidative stress and could be of therapeutic use in disorders

involving oxidative damage. The neuroprotective and radioprotective potential of arabinogalactans has been explored in studies using larch-derived arabinogalactans. These studies demonstrated antioxidant, anti-inflammatory, and immunomodulatory properties, which are consistent with our findings for Matcha-derived arabinogalactans (MAG). Qi *et al.*⁴⁹ and Liu *et al.*⁵⁰ reported that larch arabinogalactans enhance immune responses and exhibit antioxidant properties, which aligns with the observed reduction in oxidative stress markers (*e.g.*, MDA) and increased antioxidant enzyme activities (*e.g.*, SOD, GSH) in our study. MAG contains bioactive phenolic compounds, including Gallic acid and Chlorogenic acid, which have been studied extensively for their radioprotective effects. Gallic acid has been shown to scavenge free radicals and reduce lipid peroxidation, similar to the reduction in MDA levels observed in our study. Studies by Hadidi *et al.*⁵¹ highlight its anti-inflammatory properties through NF- κ B inhibition, which parallels the reduced cytokine levels (TNF- α , IL-1 β , IL-6) we observed. Chlorogenic acid is known for its neuroprotective effects via antioxidant and anti-apoptotic pathways. Zha *et al.*⁵² reported its ability to upregulate antioxidant enzymes like SOD and GSH, consistent with our findings.

These comparisons emphasize that MAG's radioprotective effects are likely synergistic, leveraging both its polysaccharide and phenolic components. When compared to a synthetic radioprotective agent such as amifostine⁵³, which is approved for clinical use, MAG is particularly effective in reducing dry mouth during radiotherapy. Its primary mechanism involves scavenging free radicals and protecting normal tissues from radiation damage. However, it has limitations, including side effects such as nausea and hypotension⁵⁴. MAG is a natural compound with oral bioavailability, making it more suitable for preclinical and possibly clinical use. Unlike amifostine, MAG's effects are multifaceted, addressing not only oxidative stress but also inflammation (*e.g.*, decreased cytokine levels) and apoptosis (*e.g.*, Bax and Bcl2)⁵⁵. While MAG does not yet match the well-documented efficacy of amifostine, its natural origin and low toxicity profile may make it a promising alternative or complementary radioprotective agent. Further direct comparisons in preclinical and clinical studies are needed to determine its relative efficacy.

It is, however, important to clarify at the outset that although our studies indicate the anti-inflammatory function of MGA in a radiation context, more studies are required to determine the exact mechanism

by which such protection may occur. Furthermore, long-term *in vivo* studies and clinical trials will be required to demonstrate efficacy and safety for the proposed use of MGA as a radioprotective drug in human populations.

Histological examination after antioxidant therapy shows its protective effect against gamma-ray-induced damage in cerebral tissues. Control groups, irrespective of the presence of antioxidants, had normal brain parenchyma with no lesions, while there was significant histological damage after exposure to gamma rays. The addition of antioxidants mitigated this damage, as revealed by a lower lesion score and improved integrity of brain tissue in the group Gamma rays + Antioxidant. These findings are therefore a testament to the effectiveness of antioxidants in maintaining cerebral health even against oxidative stress.

The study represents a preclinical investigation using a single-dose protocol in an animal model. Further studies are necessary to explore the dose-response relationship, long-term effects, and specific molecular targets of MAG, as well as its relevance in clinical settings. Although this study focused on short-term outcomes, extending observations over a longer period would help determine whether the protective effects of MAG are sustained and how they influence long-term neuroprotection. Beyond biochemical and histological assessments, future research could include behavioral and cognitive tests to comprehensively evaluate functional improvements, particularly in memory and learning.

CONCLUSION

Our study sheds light on the potential of arabinogalactans from matcha (MAG) to protect the brain from gamma radiation damage. We found that MAG appears to be a potent antioxidant. It reduced oxidative stress markers and enhanced the natural antioxidant defenses of the brain in irradiated rats. We also observed strong anti-inflammatory effects. MAG attenuated the elevation of several markers of inflammation, which are typically exacerbated after irradiation. MAG appears to help prevent cell death. It is among the proteins involved in apoptosis (programmed cell death) and can keep many brain cells alive. Interestingly, MAG also maintained BDNF levels, which are key to maintaining brain health and function. The treatment normalized several important enzymes associated with neurotransmitters normally damaged by radiation.

Upon microscopic examination of the brain tissue, we observed more damage and less inflammation in mice

treated with MAG before irradiation. Future studies should dig deeper into the exact mechanism of action of MAG and investigate its possible release from long-term adverse effects.

ABBREVIATIONS

ABTS• + (2,2'-Azino-bis(3-ethylbenzothiazoline-6-sulfonic acid)); **AChE** (Acetylcholinesterase); **AG** (Arabinogalactans); **ANOVA** (Analysis of Variance); **APP** (Amyloid Precursor Protein); **ATR** (Attenuated Total Reflectance); **BAX** (BCL2-Associated X protein); **BCL2** (B-cell lymphoma 2); **BDNF** (Brain-Derived Neurotrophic Factor); **B & A** (Pre- and Post-MAG treatment with radiation); **BSA** (Bovine Serum Albumin); **CAT** (Catalase); **cDNA** (Complementary DNA); **CE** (Catechin Equivalent); **Ct** (Threshold Cycle); **DAPI** (4',6-Diamidino-2-Phenylindole); **DPPH•** (2,2-Diphenyl-1-picrylhydrazyl); $\Delta\Delta Ct$ (Double Delta Ct); **FTIR** (Fourier Transform Infrared Spectroscopy); **GAE** (Gallic Acid Equivalent); **GSH** (Glutathione); **Gy** (Gray); **G*Power** (Statistical power analysis software); **H&E** (Hematoxylin and Eosin); **HMW** (High Molecular Weight); **HPLC** (High-Performance Liquid Chromatography); **HRP** (Horseradish Peroxidase); **IACUC** (Institutional Animal Care and Use Committee); **IL-1 β** (Interleukin 1 beta); **IL-6** (Interleukin 6); **LD50** (Lethal Dose, 50%); **MAG** (Matcha-derived Arabinogalactans); **MAO-A** (Monoamine Oxidase A); **MDA** (Malondialdehyde); **NF- κ B** (Nuclear Factor Kappa B); **NCRRT** (National Center for Radiation Research and Technology); **NIH** (National Institutes of Health); **OCT** (Optimal Cutting Temperature); **PBS** (Phosphate-Buffered Saline); **QPCR** (Quantitative Polymerase Chain Reaction); **Rad** (Radiation-only group); **RT-PCR** (Reverse Transcription Polymerase Chain Reaction); **SDS-PAGE** (Sodium Dodecyl Sulfate-Polyacrylamide Gel Electrophoresis); **SEM** (Standard Error of the Mean); **SOD** (Superoxide Dismutase); **SPSS** (Statistical Package for the Social Sciences); **TE** (Trolox Equivalent); **TFA** (Trifluoroacetic Acid); **TNF- α** (Tumor Necrosis Factor-alpha); **WB** (Western Blot); **3Rs** (Replacement, Reduction, Refinement); and **β GlcY** (β -glucosyl-Yariv reagent).

ACKNOWLEDGMENTS

The authors are grateful to Professors Mohamed Refaat and Sherein Saied Abdelgayed Department of Pathology, Faculty of Veterinary Medicine, Cairo University for his generous help in the examination of the histopathological and immunohistochemistry findings.

AUTHOR'S CONTRIBUTIONS

Dr. Mohamed Y.M. Awad performed the assays, analyzed data and drafted manuscript. Dr. Eithar K. El Adham designed the experiments, analyzed the data and wrote the manuscript. Prof. Amal I. Hassan performed the animal experiment, designed the experiments, writing& editing. All authors read and approved the final manuscript.

FUNDING

None.

AVAILABILITY OF DATA AND MATERIALS

Data and materials used and/or analyzed during the current study are available from the corresponding author on reasonable request.

ETHICS APPROVAL

Study was taken up after the approval of National Center for Radiation Research and Technology Research Ethics Committee (REC- NCRRT), (Approval No P/35A/ 24) in 02-05-2024.

CONSENT FOR PUBLICATION

Not applicable.

COMPETING INTERESTS

The authors declare that they have no competing interests.

REFERENCES

1. Saeidy S, Petera B, Pierre G, Fenoradosoa TA, Djomdi D, Michaud P. Plants arabinogalactans: from structures to physico-chemical and biological properties. *Biotechnology Advances*. 2021;53. PMID: 33992708. Available from: <https://doi.org/10.1016/j.biotechadv.2021.107771>.
2. Karki S. Phytochemicals, anti-oxidant and sensory analysis of gurjo (*tinospora sinensis*) stem incorporated green tea (*camellia sinensis*). Doctoral dissertation, Department of Food Technology Central Campus of Technology Institute of Science and Technology Tribhuvan University, Nepal 2022. Department of Food Technology Central Campus of Technology Institute of; 2022.
3. Hu T, Wu P, Zhan J, Wang W, Shen J, Wang M. Structure variety and its potential effects on biological activity of tea polysaccharides. *Food Science and Human Wellness*. 2022;11(3):587-97. Available from: <https://doi.org/10.1016/j.fshw.2021.12.015>.
4. Pariset E, Malkani S, Cekanaviciute E, Costes SV. Ionizing radiation-induced risks to the central nervous system and countermeasures in cellular and rodent models. *International Journal of Radiation Biology*. 2021;97(sup1):S132-50. Available from: <https://doi.org/10.1080/09553002.2020.1820598>.
5. Narasimhamurthy RK, Mumbreakar KD, Rao BSS. Effects of low dose ionizing radiation on the brain- a functional, cellular, and molecular perspective. *Toxicology*. 2022;465. PMID: 34774978. Available from: <https://doi.org/10.1016/j.tox.2021.153030>.

6. López-Franco YL, Higuera-Ciajara I, Lizardi-Mendoza J, Wang W, Goycoolea FM. Other exudates: tragacanth, karaya, mesquite gum, and larchwood arabinogalactan. *Handb Hydrocoll*; 2021.
7. Zakir F, Bishnoi M, Aggarwal G. Arabinogalactan-Based Drug Delivery Systems. In: Dureja, H., Adams, J., Löbenberg, R., Andreoli Pinto, T.d.J., Dua, K. (eds) *Natural Polymeric Materials based Drug Delivery Systems in Lung Diseases*. Springer, Singapore. https://doi.org/10.1007/978-981-19-7656-8_10. Springer.
8. Prescott JH, Enriquez P, Jung C, Menz E, Groman EV. Larch arabinogalactan for hepatic drug delivery: isolation and characterization of a 9 kDa arabinogalactan fragment. *Carbohydrate Research*. 1995;278(1):113–28. PMID: 8536264. Available from: [https://doi.org/10.1016/0008-6215\(95\)00241-2](https://doi.org/10.1016/0008-6215(95)00241-2).
9. Baumann A, Pfeifer L, Classen B. Arabinogalactan-proteins from non-coniferous gymnosperms have unusual structural features. *Carbohydrate Polymers*. 2021;261:117831. Available from: <https://doi.org/10.1016/j.carbpol.2021.117831>.
10. Faramarzi S, Piccolella S, Manti L, Pacifico S. Could polyphenols really be a good radioprotective strategy? *Molecules* (Basel, Switzerland). 2021;26(16):4969. PMID: 34443561. Available from: <https://doi.org/10.3390/molecules26164969>.
11. Altomare A, Fiore M, D'Ercole G, Imperia E, Nicolosi RM, Posta SD. Protective Role of Natural Compounds under Radiation-Induced Injury. *Nutrients*. 2022;14(24):5374. PMID: 36558533. Available from: <https://doi.org/10.3390/nu14245374>.
12. Huang W, Zhao M, Wang X, Tian Y, Wang C, Sun J. Revisiting the structure of arabinogalactan from *Lycium barbarum* and the impact of its side chain on anti-ageing activity. *Carbohydrate Polymers*. 2022;286. PMID: 35337529. Available from: <https://doi.org/10.1016/j.carbpol.2022.119282>.
13. Bartels D, Baumann A, Maeder M, Geske T, Heise EM, von Schwartzberg K. Evolution of plant cell wall: arabinogalactan-proteins from three moss genera show structural differences compared to seed plants. *Carbohydrate Polymers*. 2017;163:227–35. PMID: 28267501. Available from: <https://doi.org/10.1016/j.carbpol.2017.01.043>.
14. Classen B, Mau SL, Bacic A. The arabinogalactan-proteins from pressed juice of *Echinacea purpurea* belong to the hybrid class of hydroxyproline-rich glycoproteins. *Planta Medica*. 2005;71(1):59–66. PMID: 15678375. Available from: <https://doi.org/10.1055/s-2005-837752>.
15. Paulsen BS, Craik DJ, Dunstan DE, Stone BA, Bacic A. The Yariv reagent: behaviour in different solvents and interaction with a gum arabic arabinogalactan-protein. *Carbohydrate Polymers*. 2014;106:460–8. PMID: 24721102. Available from: <https://doi.org/10.1016/j.carbpol.2014.01.009>.
16. Zilić S, Serpen A, Akçulu G, Gökmen V, Vanč J. Phenolic compounds, carotenoids, anthocyanins, and antioxidant capacity of colored maize (*Zea mays* L.) kernels. *Journal of Agricultural and Food Chemistry*. 2012;60(5):1224–31. PMID: 22248075. Available from: <https://doi.org/10.1021/jf204367z>.
17. Ć S, Vanč J, Janković M, Maksimović V. Chemical composition, bioactive compounds, antioxidant capacity and stability of floral maize (*Zea mays* L.) pollen. *Journal of Functional Foods*. 2014;10:65–74. Available from: <https://doi.org/10.1016/j.jff.2014.05.007>.
18. Thi ND, Hwang ES. Bioactive compound contents and antioxidant activity in *Aronia* (*Aronia melanocarpa*) leaves collected at different growth stages. *Preventive Nutrition and Food Science*. 2014;19(3):204–12. PMID: 25320718. Available from: <https://doi.org/10.3746/pnf.2014.19.3.204>.
19. Ifeoma O, Oluwakanyinsola S. Screening of herbal medicines for potential toxicities. *New insights into Toxic drug*. *Test*. 2013;244:63–88.
20. Saganuwan SA. Toxicity studies of drugs and chemicals in animals: an overview. *Bulgarian Journal of Veterinary Medicine*. 2017;20(4):291–318. Available from: <https://doi.org/10.15547/bjvm.983>.
21. Akhila JS, Shyamjith D, Alwar MC. Current science. Acute toxicity studies and determination of median lethal dose. *Current Science*. 2007;p. 917–20. Available from: <https://www.jstor.org/stable/24099255>.
22. Lee WH, Sonntag WE, Mitschelen M, Yan H, Lee YW. Irradiation induces regionally specific alterations in pro-inflammatory environments in rat brain. *International Journal of Radiation Biology*. 2010;86(2):132–44. PMID: 20148699. Available from: <https://doi.org/10.3109/09553000903419346>.
23. Livak KJ, Schmittgen TD. Analysis of relative gene expression data using real-time quantitative PCR and the 2⁻ΔΔCT method. *Methods*. 2001;25(4):402–8. Available from: <https://doi.org/10.1006/meth.2001.1262>.
24. Kiernan J. *Histological and histochemical methods*. Scion publishing ltd; 2015.
25. Zhang X, Hartmann P. How to calculate sample size in animal and human studies. *Frontiers in Medicine*. 2023;10. PMID: 37663663. Available from: <https://doi.org/10.3389/fmed.2023.1215927>.
26. Cheng Z, Wang J, Bian Y, Tan M, Chen Y, Wang Y. Oral polysaccharide-coated liposome-modified double-layered nanoparticles containing anthocyanins: preparation, characterization, biocompatibility and evaluation of lipid-lowering activity in vitro. *Food Chemistry*. 2024;439. PMID: 38091786. Available from: <https://doi.org/10.1016/j.foodchem.2023.138166>.
27. Zhou XL, Sun PN, Bucheli P, Huang TH, Wang D. FT-IR methodology for quality control of arabinogalactan protein (AGP) extracted from green tea (*Camellia sinensis*). *Journal of Agricultural and Food Chemistry*. 2009;57(12):5121–8. PMID: 19456132. Available from: <https://doi.org/10.1021/jf803707a>.
28. Mohammadipour M, Karbasi S, Behzad T, Mohammadipour Z, Zamani M. Effect of cellulose nanofibers on polyhydroxybutyrate electrospun scaffold for bone tissue engineering applications. *International Journal of Biological Macromolecules*. 2022;220:1402–14. PMID: 36116594. Available from: <https://doi.org/10.1016/j.ijbiomac.2022.09.118>.
29. Sudatta BP, Sugumar V, Varma R, Nigariga P. Extraction, characterization and antimicrobial activity of chitosan from pen shell, *Pinna bicolor*. *International Journal of Biological Macromolecules*. 2020;163:423–30. PMID: 32629046. Available from: <https://doi.org/10.1016/j.ijbiomac.2020.06.291>.
30. Sultan M, Elsayed H, Abdelhakim AE, Taha G. Active packaging gelatin films based on chitosan/Arabic gum/coconut oil Pickering nano emulsions. *Journal of Applied Polymer Science*. 2022;139(1):51442. Available from: <https://doi.org/10.1002/app.51442>.
31. Musa C, Zaidi M, Depriester M, Allouche Y, Naouar N, Bourmaud A. Development of foam composites from flax gum-filled epoxy resin. *Journal of Composites Science*. 2024;8(7):244. Available from: <https://doi.org/10.3390/jcs8070244>.
32. Wu J, Xu Y, Zhu B, Liu K, Wang S, Sheng Y. Characterization of an arabinogalactan from the fruit hulls of *Ficus pumila* Linn. and its immunomodulatory effect. *Journal of Functional Foods*. 2020;73. Available from: <https://doi.org/10.1016/j.jff.2020.104091>.
33. Wudali SN, Barwad A, Banadka A, Shaikh A, Al-Khayri JM, Nagella P. Bioactive Compounds and Biological Activities of Taro (*Colocasia esculenta* L.). Schott. Springer; 2023. Available from: https://doi.org/10.1007/978-3-031-29006-0_2-1.
34. Wang K, Zhou Y, Li M, Chen Z, Wu Z, Ji W. Structural elucidation and immunomodulatory activities in vitro of type I and II arabinogalactans from different origins of *Astragalus membranaceus*. *Carbohydrate Polymers*. 2024;333. PMID: 38494227. Available from: <https://doi.org/10.1016/j.carbpol.2024.121974>.
35. Li X, Chen Q, Liu G, Xu H, Zhang X. Chemical elucidation of an arabinogalactan from rhizome of *Polygonatum sibiricum* with antioxidant activities. *International Journal of Biological Macromolecules*. 2021;190:730–8. PMID: 34520778. Available from: <https://doi.org/10.1016/j.ijbiomac.2021.09.038>.

36. Fan X, Xiao X, Yu W, Yu B, He J, Zheng P. Yucca schidigera purpurea-sourced arabinogalactan polysaccharides augments antioxidant capacity facilitating intestinal antioxidant functions. *Carbohydrate Polymers*. 2024;326. PMID: 38142074. Available from: <https://doi.org/10.1016/j.carbpol.2023.121613>.
37. Desai RI, Limoli CL, Stark CE, Stark SM. Impact of spaceflight stressors on behavior and cognition: A molecular, neurochemical, and neurobiological perspective. *Neuroscience and Biobehavioral Reviews*. 2022;138. PMID: 35461987. Available from: <https://doi.org/10.1016/j.neubiorev.2022.104676>.
38. Venkidesh BS, Narasimhamurthy RK, Jnana A, Reghunathan D, Sharan K, Chandraguthi SG. Pelvic irradiation induces behavioural and neuronal damage through gut dysbiosis in a rat model. *Chemico-Biological Interactions*. 2023;386. PMID: 37866488. Available from: <https://doi.org/10.1016/j.cbi.2023.110775>.
39. Glushakova OY, Glushakov AO, Borlongan CV, Valadka AB, Hayes RL, Glushakov AV. Role of caspase-3-mediated apoptosis in chronic caspase-3-cleaved tau accumulation and blood brain barrier damage in the corpus callosum after traumatic brain injury in rats. *Journal of Neurotrauma*. 2018;35(1):157-73. PMID: 28637381. Available from: <https://doi.org/10.1089/neu.2017.4999>.
40. Yang J, Gao J, Han D, Li Q, Liao C, Li J. Hippocampal changes in inflammasomes, apoptosis, and MEMRI after radiation-induced brain injury in juvenile rats. *Radiation Oncology (London, England)*. 2020;15(1):78. PMID: 32276638. Available from: <https://doi.org/10.1186/s13014-020-01525-3>.
41. Fang D, Wang H, Li M, Wei W. α -bisabolol enhances radiotherapy-induced apoptosis in endometrial cancer cells by reducing the effect of XIAP on inhibiting caspase-3. *Bio-science Reports*. 2019;39(6). PMID: 31127027. Available from: <https://doi.org/10.1042/BSR20190696>.
42. Jia G, Zhang Y, Li W, Dai H. Neuroprotective role of icariin in experimental spinal cord injury via its antioxidant, anti-neuroinflammatory and anti-apoptotic properties. *Molecular Medicine Reports*. 2019;20(4):3433-9. PMID: 31432160. Available from: <https://doi.org/10.3892/mmr.2019.10537>.
43. Zhang Q, Wei S, Lu J, Fu W, Chen H, Huang Q. Necrostatin-1 accelerates time to death in a rat model of cecal ligation and puncture and massively increases hepatocyte caspase-3 cleavage. *American Journal of Physiology Gastrointestinal and Liver Physiology*. 2019;316(4):551-61. PMID: 30735454. Available from: <https://doi.org/10.1152/ajpgi.00175.2018>.
44. Khan MZ, Khan A, Chen W, Chai W, Wang C. Advancements in Genetic Biomarkers and Exogenous Antioxidant Supplementation for Safeguarding Mammalian Cells against Heat-Induced Oxidative Stress and Apoptosis. *Antioxidants*. 2024;13(3):258. PMID: 38539792. Available from: <https://doi.org/10.3390/antiox13030258>.
45. Najafi M, Motevaseli E, Shirazi A, Geraily G, Rezaeyan A, Norouzi F. Mechanisms of inflammatory responses to radiation and normal tissues toxicity: clinical implications. *International Journal of Radiation Biology*. 2018;94(4):335-56. PMID: 29504497. Available from: <https://doi.org/10.1080/09553002.2018.1440092>.
46. Wei J, Wang B, Wang H, Meng L, Zhao Q, Li X, et al. Radiation-induced normal tissue damage: oxidative stress and epigenetic mechanisms. *Oxidative medicine and cellular longevity*. 2019;2019(1):3010342. Available from: <https://doi.org/10.1155/2019/3010342>.
47. Bai J, Zhang Y, Tang C, Hou Y, Ai X, Chen X. Gallic acid: pharmacological activities and molecular mechanisms involved in inflammation-related diseases. *Biomedicine and Pharmacotherapy*. 2021;133. PMID: 33212373. Available from: <https://doi.org/10.1016/j.biopha.2020.110985>.
48. Zhang Y, Huang Y, Li Z, Wu H, Zou B, Xu Y. Exploring Natural products as Radioprotective agents for Cancer Therapy: mechanisms, challenges, and opportunities. *Cancers (Basel)*. 2023;15(14):3585. PMID: 37509245. Available from: <https://doi.org/10.3390/cancers15143585>.
49. Qi H, Tang S, Bian B, Lai C, Chen Y, Ling Z. Effect of H2O2-VC degradation on structural characteristics and immunomodulatory activity of larch arabinogalactan. *Frontiers in Bioengineering and Biotechnology*. 2024;12. PMID: 39170060. Available from: <https://doi.org/10.3389/fbioe.2024.1461343>.
50. Liu Y, Liu Q, Ma M, Zhang J, Liu M, Mosenthin R. Dietary arabinogalactan modulates immunity and improves gut barrier in broilers via regulating metabolome and gut microbiome. *Carbohydrate Polymers*. 2025;352. PMID: 39843118. Available from: <https://doi.org/10.1016/j.carbpol.2025.123223>.
51. Hadidi M, Liñán-Atero R, Tarahi M, Christodoulou MC, Aghababaei F. The potential health benefits of gallic acid: therapeutic and food applications. *Antioxidants*. 2024;13(8):1001. PMID: 39199245. Available from: <https://doi.org/10.3390/antiox13081001>.
52. Zha P, Wei L, Liu W, Chen Y, Zhou Y. Effects of dietary supplementation with chlorogenic acid on growth performance, antioxidant capacity, and hepatic inflammation in broiler chickens subjected to diquat-induced oxidative stress. *Poultry Science*. 2023;102(3). PMID: 36669355. Available from: <https://doi.org/10.1016/j.psj.2023.102479>.
53. Ji L, Cui P, Zhou S, Qiu L, Huang H, Wang C. Advances of amifostine in radiation protection: administration and delivery. *Molecular Pharmaceutics*. 2023;20(11):5383-95. PMID: 37747899. Available from: <https://doi.org/10.1021/acs.molpharmaceut.3c00600>.
54. Wu M, Wu K, Chen P, Li P, Xie Y. Administration of amifostine in the stage of remission induction can benefit the patients with hematological malignancy in autologous stem cell transplantation: a retrospective study. *Translational Cancer Research*. 2020;9(9):5147-54. PMID: 35117881. Available from: <https://doi.org/10.21037/tcr-20-1366>.
55. Cai L, Gan M, Regenstein JM, Luan Q. Improving the biological activities of astaxanthin using targeted delivery systems. *Critical Reviews in Food Science and Nutrition*. 2024;64(20):6902-23. PMID: 36779336. Available from: <https://doi.org/10.1080/10408398.2023.2176816>.